CPP

Contributions to Plasma Physics

www.cpp-journal.org

WILEY-VCH

REPRINT

Contrib. Plasma Phys. **51**, No. 4, 361 – 366 (2011) / **DOI** 10.1002/ctpp.201010103

Interaction of Short Laser Pulses in Wavelength Range from Infrared to X-ray with Metals, Semiconductors, and Dielectrics

N. A. Inogamov * [1], **A. Ya. Faenov**[2,3], **V. V. Zhakhovskii**[2,4], **I. Yu. Skobelev**[2], **V. A. Khokhlov**[1], **Y. Kato**[5,3], **M. Tanaka**[3], **T. A. Pikuz**[2,3], **M. Kishimoto**[3], **M. Ishino**[3], **M. Nishikino**[3], **Y. Fukuda**[3], **S. V. Bulanov**[3], **T. Kawachi**[3], **Yu. V. Petrov**[1], **S. I. Anisimov**[1], and **V. E. Fortov**[2]

[1] Landau Institute for Theoretical Physics, Russian Academy of Sciences, Chernogolovka 142432, Russia
[2] Joint Institute for High Temperatures, Russian Academy of Sciences, Moscow 125412, Russia
[3] Kansai Photon Science Institute, Japan Atomic Energy Agency, Kyoto 619-0215, Japan
[4] Institute of Laser Engineering, Osaka University, Osaka 565-0871, Japan
[5] The Graduate School for the Creation of New Photonics Industries, Hamamatsu, Shizuoka 431-1202, Japan

Received 14 September 2009, revised 07 December 2009, accepted 10 January 2010
Published online 4 May 2010

Key words Spallative ablation by optical and X-ray lasers, two-temperature warm dense matter.

Laser-matter interaction is defined by an electronic band structure of condensed matter and frequency ω_L of electromagnetic radiation. In the range of moderate fluences, the energy absorbed by electrons from radiation finally thermalizes in the ion thermal energy. The thermalization processes are different for optical as compared with X-ray quanta and for metals relative to semiconductors and dielectrics, since the light absorption and electron-electron, electron-ion dynamics are sensitive to the electron population in a conduction band and the width of a forbidden gap. Although the thermalization processes are different, the final state is simply a heated matter. Laser heating creates powerful stresses in a target if duration of a laser pulse τ_L is short in acoustic time scale. Nucleation and material removal take place under such stresses. Such way of removal is called here the spallative ablation. Thus the spallative ablation is an ablation mechanism universally important for qualitatively different materials and quanta.

Laser-matter interaction is a great fundamental issue of high significance for many industrial applications. Usually it is divided into several scientific directions depending on wavelength, pulse duration, and material properties because the physics of absorption and electron-electron, electron-ion interactions are sensitive to these parameters. Here we want to attract attention to the universal feature which controls material removal for various wavelengths and materials if the pulse duration τ_L is short. This is the spallative ablation which should take place in any case (i) when the delivery of laser energy is faster than elastic reaction to heating and, (ii) the absorbed energy density is comparable to the cohesive energy of condensed state. Why is this so?

Atoms - a system of an ion and electrons - interact with radiation through electron subsystem. Therefore absorbed laser energy should pass through electrons. For moderate and large absorbed fluences F_{abs} the electron-electron thermalization is fast. Hot electrons transfer the absorbed energy to heavy particles by means of electron-phonon collisions, in case of crystal, and through electron-ion interactions, in case of amorphous solids and melts. The rate of these collisions defines time t_{eq} necessary for electron-ion equilibration.

There are three time scales: τ_L, t_{eq}, and t_s, where $t_s = d_T/c_s$ or $t_s = d_f/c_s$ shows how fast is acoustic response to laser irradiation, d_T is a heat penetration depth, d_f is the thickness of a foil target. It is replaced by d_T if a foil is thinner than the heat penetration depth $d_f < d_T$, and c_s is sonic velocity. Laser pulse increases pressure in the heated layer d_T or in a thin foil d_f from $p = 0$ to p_{load}. For short pulses

$$\tau_L < t_s \tag{1}$$

this increase p_{load} is of the order of volume density F_{abs}/d_T of absorbed energy because the Gruneisen factor Γ is of the order of unity.

* Corresponding author: E-mail: nailinogamov@googlemail.com, Phone: +07 495 425 8767; Fax: +07 495 702 9317

Electron Γ_e and ion Γ_i numbers are both of the same order, regardless of the fact that the electrons are degenerate, as in metals, or they are classical or semiclassical, as in semiconductors and dielectrics excited by laser pulse. Therefore it may be either

$$t_{eq} < t_s, \tag{2}$$

or

$$t_s < t_{eq} \tag{3}$$

particular case does not influence the conclusion that $p_{load} \sim F_{abs}/d_T$ or $p_{load} \sim F_{abs}/d_f$ in the case when the condition (1) takes place.

But the cases (2) and (3) are physically different. If condition (2) holds, then ion pressure p_i drives expansion at the hydrodynamical stage, while in the opposite case (3), electron pressure p_e is higher and hence its action expands matter during the time interval $t \sim t_s$.

Absorption and thermalization depend on a band structure, a room temperature electron energy distribution, and changes in this distribution during heating by laser pulse and after the end of the pulse. This is why the physical pictures vary from (i) optical quanta $\hbar\omega_L \sim 1$ eV and metals to (ii) $\hbar\omega_L \sim 1$ eV and semiconductors, (iii) $\hbar\omega_L \sim 1$ eV and dielectrics, and X-rays quanta in (iv) metals, (v) semiconductors, and (vi) dielectrics. In (i) there are [a] intra- and interband absorption by conductivity and valency electrons, [b] widening of the heated layer as a result of electron heat conduction, and [c] electron-ion energy transfer from conduction band hot electrons to ions [1,2]. At later stages, the nucleation inside the stretched melt, foam formation, and spallation take place. This explains the observations of dynamical Newton rings found in the experiments [3-7].

In (ii), there is nonlinear absorption, depending on ratio of the number of electrons in conduction band to the number of electrons necessary to increase plasma frequency up to laser frequency ω_L. This ratio depends on intensity and time after beginning of laser irradiation, because irradiation excites electrons from valence to conductivity band through direct interband transition, multi-photon, and tunnel processes. Absorption depth drops and the absorbed laser power per unit volume increases sharply after achieving the critical density of conduction electrons. At this stage, the situation with semiconductors becomes similar to that with metal. In semiconductors, the forbidden gap is narrow in comparison with dielectrics, therefore not as much energy is needed to transfer semiconductor into this stage - semiconductor is not very hot, and cohesion bonds remains dynamically significant. These reasons cause similar dynamical behavior of semiconductors at late stages with nanospallation, foaming of melt, appearance of the Newton rings, and decrease of reflection coefficient due to the foaming [7,8].Development of foam and freezing of nano-relief are the bases for formation of weakly reflecting black gold and platinum [9,10].All these phenomena provide bright manifestations of spallative ablation.

In case (iii) of dielectrics and optical irradiation, the gap is wide. Therefore, after achieving the stage with critical number of electrons in conduction band, dielectrics transform into hot state where the cohesion bonds are insignificant. Space expansion from this stage progresses as gas expansion. This means that in dielectrics the optical breakdown threshold F_{bd} is higher than the spallative ablation threshold F_{abl} introduced below. The threshold F_{abl} is determined by strength of the bonds. While in semiconductors $F_{bd} < F_{abl}$, and spallation exists.

Absorption and atomic physics of electron-ion thermalization for X-ray lasers (XRL) in cases (iv), (v), and (vi) are different from optical lasers. The initial stages are similar in the cases (iv)-(vi). High reflection of incident light, like in case of metals, is absent - all X-ray quanta are absorbed in bulk targets. There is no highly nonlinear phenomena like sharp increase of opacity during pulse as a result of accumulation of critical electron density. On the contrary, nonlinear X-ray opacity may decrease during laser pulse due to the devastation of the electron shell which are mainly absorbing XRL quanta [11,12]. But this relates to the high fluence irradiation. In our case with energetic XRL photons $\hbar\omega_L = 89.3$ eV (Ag XRL and similar devices [13-16]),and even higher X-ray photons of up to $10 - 15$ keV (XFEL [17]), concentration of excited atoms is small and nonlinear effects are negligible, because we are interested in spallation when the average energy per atom E_{abs} is of the order of cohesion energy E_{coh}. Scale of this energy is moderate even for substances with strong bonds. For metals it is of the order of $3 - 4$ eV/atom.

It is shown in this paper, that in spite of obvious differences in absorption and electron-ion relaxation stages, final stage is similar for all cases (i), (ii) and (iv)-(vi) if condition (1) holds. Absorption elevates pressure p_{load}

in the heated layer d_T. The release of this pressure into the vacuum side, in case of the targets irradiated from the vacuum boundary, creates negative pressure (tensile stress) in the stretched matter. Stretching is caused by expansion of suddenly (at acoustic time scale t_s) heated matter. Let p_{neg} be the absolute value of maximum tensile stress achieved at given irradiation fluence F. There is a strength limit p_{lim} called the material strength. It exists due to finite strength of cohesive bonds between atoms. If p_{neg} overcomes p_{lim}, then nucleation and spallation take place. This means that there is a sharp spallative ablation threshold F_{abl}, $p_{neg}(F_{abl}) = p_{lim}$, because the function $p_{neg}(F)$ grows with F.

In this picture, particular evolution at the initial stages (absorption, e-i interaction) is not significant. In any case (i), (ii), (iv)-(vi), they produce strained (or "loaded") state, negative pressures, and above the ablation threshold F_{abl} - nucleation and spallation.

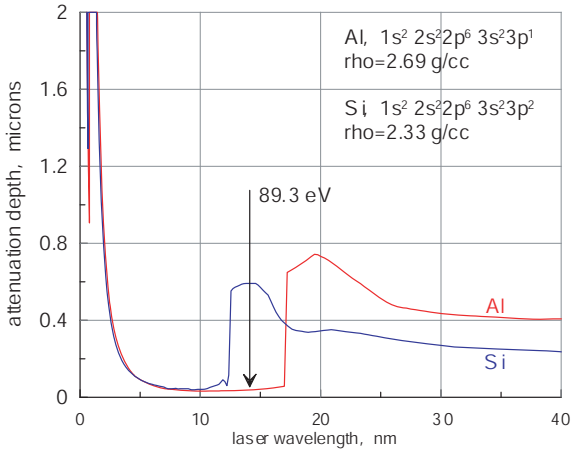

Fig. 1 Photon energy of Ag X-ray laser is between the L-edges for Al and Si. Therefore the attenuation depths for Al (37 nm) and Si (590 nm) are very different. The data is taken from [18]. (Online colour: www.cpp-journal.org).

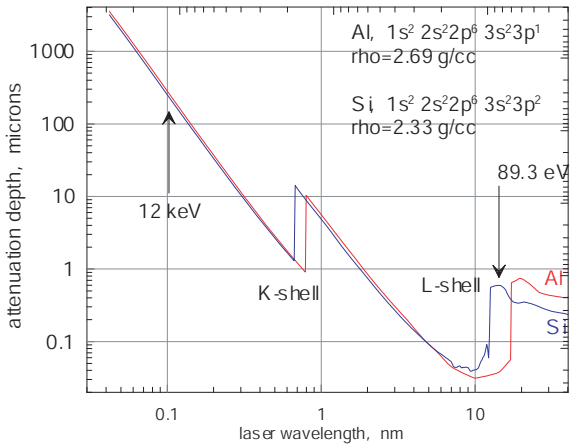

Fig. 2 Attenuation depth varies in a wide range depending on photon energy of particular X-ray laser. For high energy photons, generated by future free-electron lasers [17], this depth is large. (Online colour: www.cpp-journal.org).

Typical attenuation depths d_{att} are shown in Fig. 1 and 2. The dependencies $d_{att}(\omega_L)$ are complicated, reflecting the electron shell structure of atom. We see how large is the depth d_{att} in case of high energy quanta. Corresponding acoustic responses are also very long, because heating is moderate, and changes of sonic velocity in comparison with its room temperature values are small. E.g., for $\hbar\omega_L = 12$ keV it is $t_s = d_{att}/c_s = 30$ ns. This time is huge in comparison with picosecond time scale of e-i relaxation process. The fluence necessary to achieve spallative ablation threshold is

$$F_{abl} = k_{lim}\, d_{att}\, n_{at}\, E_{coh} \approx 200\ \mathrm{J/cm^2},$$

where $k_{lim} = 0.2 - 0.4$ is a coefficient connecting delivered laser energy and limiting strength of material [19,20], this coefficient is significantly below unity, n_{at} is atom concentration in solid state.

Future XFEL lasers [17] will have $0.1\ \mathrm{keV} < \hbar\omega_L < 12\ \mathrm{keV}$ photons, ultrashort durations $\tau_L \sim 20$ fs, and fluence up to several hundred J/cm^2. Irradiation by such a pulse can cause spallative ablation of huge sub-millimeter piece of condensed target. Three-dimensional effects will become significant as focal spot diameter d_{sp} is usually from tens to hundreds of microns. In the case when $d_{sp} < d_{att}$ powerful lateral shocks will be produced, propagating in radial directions to the heated cylinder created by pulse in a target. The length of the cylinder is $\sim d_{att}$ and its diameter is d_{sp}. Let us also mention, that in the thin surface layer (thin in comparison with d_{att}), nonlinear effects with devastation of electron shells will be significant at such high intensities of X-ray flux (large fluence, small duration).

At such laser parameters, there are little differences between cases (iv), (v), and (vi), because an additional widening Δd_{ehc} of the heated volume due to electron heat conduction is small in comparison with d_{att}. In one-temperature metals, heat diffusivity and thermal penetration are $\chi \sim 1\ \mathrm{cm^2/\,s}$ and $\Delta d_{ehc} \approx \sqrt{\chi\, t_s} \sim 2$ um $\ll d_{att}$. The same may be said about carriers and heat expansions in semiconductors and dielectrics.

Let us consider ablation flow initiated by action of Ag XRL on dielectric LiF. One dimensional approximation is valid because the diameter d_{sp} is much larger than the depth $d_{att} = 28$ nm for quanta 89.3 eV in LiF [18]. Pulse duration is $\tau_L = 7$ ps. Equations for electron concentration n_e in the conduction band and for electron total energy E_e^s are

$$\dot{n}_e = \frac{Q_L}{u_{i2}} + \nu_{imp} n_e - \kappa_{rec} n_e^3, \quad \dot{E}_e^s = Q_L - \dot{E}_{ea}, \quad Q_L = \frac{F\, e^{-t^2/\tau_L^2}}{\sqrt{\pi} d_{att} \tau_L}, \quad E_e^s = n_e u_{i2} + E_e. \tag{4}$$

Quantities n_e and E_e^s are averaged over the depth d_{att}. Simulations begin at initial instant $t_0 = -5\,\tau_L$. In (4) the Maxwellian distribution for electrons over energy is used because the e-e exchange is fast, $E_e = (3/2) n_e T_e$ is electron thermal energy, Q_L is a XRL source, F is fluence of laser, typical fluences are $F \sim 10$ mJ/cm^2, ν_{imp} and κ_{rec} are the electron impact ionization frequency and the coefficient of three-body recombination taken from [21]. In (4) the term $\dot{E}_{ea} = A\, E_e$ gives loses of energy by electron subsystem. This energy transfers from electrons to atoms. Calculations give $A \approx 1.5 \times 10^{12}$ s^{-1} for the electron-atoms exchange coefficient. Potential energy of primary ions created by XRL photons is $u_{i1} \sim 30 - 60$ eV, $u_{i2} \approx 10$ eV is the potential energy of secondary ions. The secondary ions appear as a result of impact and Auger ionizations.

Numerical integration of system (4) gives time-dependent power $E_{ea}(t)$ heating atomic subsystem. We write $E_{ea}^{loc}(x,t) = (2/\sqrt{\pi}) E_{ea}(t)\, e^{-x^2/d_{att}^2}$ for the local value of energy transfer to atoms. This power is used as energy source in our molecular dynamics (MD) simulations because in dielectrics thermal conductivity and diffusion during acoustic relaxation time t_s are small - ionized electrons and their heat are localized inside the layer d_{att}. The goal of these MD simulations is to estimate maximum negative pressure p_{neg} in a target created by our XRL laser pulse. We neglect dynamical influence of electronic pressure, as estimates show that it is small. New EAM (embedded atom methods) potential for aluminum [19] is applied because careful comparison of LiF and Al equations of states shows that they are very close to each other.

Results of MD simulations are shown in Figs. 3 and 4. Temperature profiles are estimated from temperatures for Al, taking into account double the heat capacity of LiF. But calculations are done with Al EAM potential. They show melting. For LiF the melting temperature is higher, while its temperatures are lower (since heat capacity of LiF is larger than for Al). Therefore LiF does not melt in our range of fluences ~ 10 mJ/cm^2. Melting of Al takes small amount of total absorbed energy and almost does not influence dynamics. Temperatures slightly decrease behind the melting front. The melting front is located near the small temperature drop seen in the profile for $t = 25$ ps in Fig. 4. Thickness of the molten layer is 10 nm. Decrease of temperature due to adiabatic expansion is small, because pressure drops sharply with decreasing density. The density expansion is small, thus the work done for expansion is small.

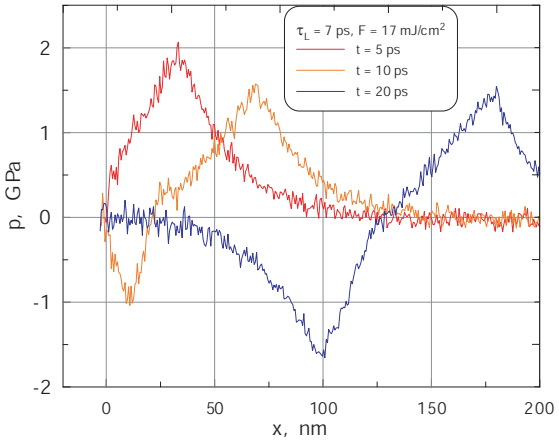

Fig. 3 Evolution of pressure profiles created due to absorption of XRL pulse. Gradually negative pressures appears. (Online colour: www.cpp-journal.org).

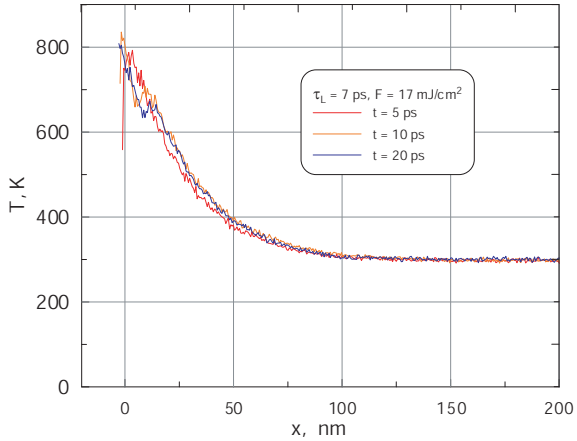

Fig. 4 Contrary to the pressure profiles, the temperature profiles remain frozen into matter. (Online colour: www.cpp-journal.org).

Main results of MD simulations concerns stress fields. Negative pressure p_{neg} gradually develops as a result of the acoustic reflection from the boundary with vacuum of the pressure perturbation created by laser heating.

The maximum value of $p_{neg} \sim 1$ GPa is achieved at the time interval 15-20 ps, and at the depth ≈ 50 nm. During further evolution p_{neg} remains constant. Therefore, near the spallative ablation threshold, the depth of a crater is 50 nm. This value agree with our experimental measurements.

The experiment has been performed with the Ne-like Ag soft X-ray laser facility at JAEA Kansai Photon Science Institute, working at transient collisional scheme [22-24]. The X-ray laser beam with the energy $\sim 1\mu$J and the horizontal and vertical divergences of 12 mrad $\times$ 5 mrad, respectively, was focused on a LiF crystal of 2 mm thickness and 20 mm diameter, by using a spherical Mo/Si multilayer mirror of 1050 mm radius of curvature. The total energy on the LiF crystal of the XRL beam, after passing 200 nm Zr filter, and reflecting from the focusing mirror, was ~ 170 nJ in a single shot. The luminescence of the stable color centers (CCs) [25-28], formed by XRL radiation, was used to measure the intensity distribution in the XRL laser focal spot [23,24]. After irradiation of the LiF crystal with the XRL, the photo-luminescence patterns from the color centers (CCs) in LiF were observed by using a confocal fluorescence laser microscope (OLYMPUS model FV300). An OLYMPUS BX60 microscope in the visible differential mode and an atomic force microscope (AFM, TOPOMETRIX Explorer), operated in the tapping mode, have been used for measurements of the size of the ablation spot. As it was shown in our previous experiments [23], only about 6% of full laser energy is concentrated to the best focus spot of $\sim 200\mu\,\mathrm{m}^2$, which corresponds to the energy of $\sim 5\,\mathrm{mJ/cm}^2$ or laser intensity $\sim 7 \times 10^8\,\mathrm{W/cm}^2$.

Two types of experimental investigations of the XRL ablation threshold of the LiF crystals were done. In the first experiments, Zr filter has been removed. Therefore, the XRL beam expands freely and then is focused on the surface of LiF crystal. Ablation of crystal materials is clearly seen from the AFM image and traces. Since the energy of the XRL beam is 350 nJ in these experiments, we can estimate the XRL laser energy threshold of the LiF crystal as $\sim 10.2\,\mathrm{mJ/cm}^2$. From the traces, we can see that the ablation depths vary between 30 and 55 nm, which is close to the absorption depth ~ 28 nm for 13.9 nm radiation [18]. In the second type of experiment, Zr filter was settled inside the XRL beam propagation path, and 3 shots were done in the same focusing spot with the fluence of $5\,\mathrm{mJ/cm}^2$. In this case a crater, with an ablation depth of about 50 nm, appears on the surface of the crystal, which is similar to the craters obtained in the previous experiments with the single more intense XRL shot. It is necessary to mention, that the ablation spot would have never been observed if only single shot with fluence $5\,\mathrm{mJ/cm}^2$ has been made. The value of the ablation threshold, obtained in our experiments, is much lower as compared with the previous experiments with the longer XRL pulse.

Acknowledgements Work of NAI, VVZh, VAK, and YuVP has been supported by the RFBR grant No. 09-08-00969-a. This research has been partially supported by the Japan Ministry of Education, Science, Sports and Culture, Grant-in-Aid for Kiban A No 20244065, Kiban B No. 21360364., by the RFBR grant No. 09-02-92482-MNKS-a (AYaF, IYuS, TAP), and by the RAS Presidium Program of basic researches No. 27.

References

[1] N. A. Inogamov, V. V. Zhakhovskii et al., Appl. Surf. Sci., doi:10.1016/j.apsusc.2009.04.139 (2009); arXiv:0812.2965 [physics.optics].
[2] W.-L. Chan, R. S. Averback, D. G. Cahill, A. Lagoutchev, Phys. Rev. B **78,** 214107 (2008).
[3] K. Sokolowski-Tinten, J. Bialkowski, A. Cavalleri, et al., Phys. Rev. Lett. **81,** 224 (1998).
[4] N. A. Inogamov, Yu. V. Petrov, S. I. Anisimov, et al., JETP Lett. **69,** 310 (1999).
[5] V. V. Zhakhovski, K. Nishihara, S. I. Anisimov, N. A. Inogamov, JETP Lett. **71,** 167 (2000).
[6] D. von der Linde, K. Sokolowski-Tinten, Appl. Surf. Sci. **154-155,** 1 (2000).
[7] N. A. Inogamov, V. V. Zhakhovskii, S. I. Ashitkov, et al., JETP **107,** 1 (2008).
[8] J. Bonse, G. Bachelier, J. Siegel, J. Solis, H. Sturm, J. Appl. Phys. **103,** 054910 (2008).
[9] V. V. Zhakhovskii, N. A. Inogamov, K. Nishihara, JETP Lett. **87,** 423 (2008).
[10] A. Y. Vorobyev, C. Guo, Appl. Phys. Lett. **92,** 041914 (2008).
[11] B. Nagler, U. Zastrau, R.R. Faeustlin, S.M. Vinko, T. Whitcher, et al., Nature Phys. **5** 693 (2009); www.nature.com/naturephysics
[12] M. Bergh, N. Tmneanu, S. P. Hau-Riege, H. A. Scott, Phys. Rev. E **77,** 026404 (2008).
[13] J. Dunn, Y. Li, A. L. Osterheld, et al., Phys. Rev. Lett. **84,** 4834 (2000).
[14] M. Tanaka, M. Nishikino, T. Kawachi, et al., Opt. Lett. **28,** 1680 (2003).
[15] S. Heibuch, M. Grisham, D. Martz, J. J. Rocca, Opt. Express **13,** 4050 (2005).
[16] Y. Wang, M. A. Larotonda, B. M. Luther, et al., Phys. Rev. A **72,** 053807 (2005).
[17] http://www.xfel.eu/; http://www.riken.jp/XFEL/eng/index.html

[18] http://henke.lbl.gov/optical_constants/
[19] V. V. Zhakhovskii, N. A. Inogamov, et al. Appl. Surf. Sci., doi:10.1016/j.apsusc.2009.04.082 (2009).
[20] A. K. Upadhyay, N. A. Inogamov, B. Rethfeld, H. M. Urbassek, Phys. Rev. B **78,** 045437 (2008).
[21] L. M. Biberman, V. S. Vorobyev, I. T. Yakubov, "Kinetics of Nonequilibrium Low-Temperature Plasmas" (Springer, Berlin, 1987); I. I. Sobelman, L. A. Vainshtein, E. A. Yukov, "Excitation of Atoms and Broadening of Spectral Lines" (Springer Series on Atoms and Plasma), Springer, April 2007.
[22] M. Nishikino, N. Hasegawa, T. Kawachi, H. Yamatani, K. Sukegawa, K. Nagashima, Applied Optics **47**, 1129 (2008).
[23] A. Ya. Faenov, Y. Kato, M. Tanaka, T. A. Pikuz, M. Kishimoto, M. Ishino, M. Nishikino, Y. Fukuda, S. V. Bulanov, T. Kawachi, Optic Letters **34**, 941 (2009).
[24] A. Ya. Faenov, N. A. Inogamov, V. V. Zhakhovskii, V. A. Khokhlov, K. Nishihara, Y. Kato , M. Tanaka, T. A. Pikuz, M. Kishimoto, M. Ishino, M. Nishikino, T. Nakamura, Y. Fukuda, S. V. Bulanov, T. Kawachi, Applied Phys. Lett. **94**, 231107 (2009).
[25] G. Baldacchini, S. Bollanti, F. Bonfigli, P. Di Lazzaro, A. Ya. Faenov, F. Flora, T. Marolo, R. M. Montereali, D. Murra, E. Nichelatti, T. Pikuz, A. Reale, L. Reale, A. Ritucci, G. Tomassetti, IEEE Journal of Selected Topics in Quantum Electronics **10**, 1435 (2004)
[26] G. Baldacchini, S. Bollanti, F. Bonfigli, F. Flora, P. Di Lazzaro, A. Lai, T. Marolo, R. M. Montereali, D. Murra, A. Faenov, T. Pikuz, E. Nichelatti, G. Tomassetti, A. Reale, L. Reale, A. Ritucci, T. Limongi, L. Palladino, M. Francucci, S. Martellucci, G. Petrocelli, Rev. Sci. Instrum. **76**, 113104 (2005).
[27] A. Ustione, A. Cricenti, F. Bonfigli, F. Flora, A. Lai, T. Marolo, R. M. Montereali, G. Baldacchini, A. Faenov, T. Pikuz, L. Reale, Appl. Phys. Lett. **88**, 141107 (2006).
[28] G. Tomassetti, A. Ritucci, A. Reale, L. Palladino, L. Reale, L. Arrizza, G. Baldacchini, F. Bonfigli, F. Flora, L. Mezi, R. M. Montereali, S. V. Kukhlevsky, A. Faenov, T. Pikuz, J. Kaiser, Europhys. Lett. **63**, 681 (2003).

